minerals

MDPI

Article

Upper Paleozoic Transitional Shale Gas Enrichment Factors: A Case Study of Typical Areas in China

Feiteng Wang [1,2] and Shaobin Guo [1,2,*]

[1] School of Energy Resource, China University of Geosciences (Beijing), Beijing 100083, China; feiteng.wang@outlook.com

[2] Key Laboratory of Strategy Evaluation for Shale Gas, Ministry of Land and Resources, Beijing 100083, China

* Correspondence: guosb58@cugb.edu.cn

Received: 28 January 2020; Accepted: 18 February 2020; Published: 20 February 2020

Abstract: Based on the shale gas research experience in North America, large-scale geological evaluations have been conducted in China to determine the enrichment characteristics of deep marine shale gas, leading to the discovery of the Fuling, Changning and Weiyuan shale gas fields. However, research on Upper Paleozoic transitional shale gas remains limited, restricting the subsequent exploration and development. Therefore, taking the Lower Permian Shanxi and Pennsylvanian Taiyuan Formations in the northeastern Ordos Basin and the Upper Permian Longtan Formation in southwestern Guizhou as examples, gas logging, gas desorption, thermal simulation, maximum vitrinite reflectance (Rmax), and X-ray diffraction (XRD) were used to study the influence of lithological associations, sedimentary facies, gas generation thresholds, and pore evolution on transitional shale gas, and then Upper Paleozoic transitional shale gas enrichment factors of the northeastern Ordos Basin and southwestern Guizhou were analysed. The results show that carbonaceous mudstone adjacent to coal seams presents a high gas content level, and is primarily developed in swamps in the delta plain environment, and swamps and lagoons in the barrier coastal environment. The gas generation threshold maturity (Rmax) of transitional shale is 1.6% and the corresponding threshold depths of the northeastern Ordos Basin and southwestern Guizhou are estimated to be 2265 m and 1050 m. Transitional shale pore evolution is jointly controlled by hydrocarbon generation, clay minerals transformation, and compaction, and may have the tendency to decrease when Rmax < 1.6% or Rmax > 3.0%, but increase when Rmax ranges between 1.6% and 3.0%, while the main influential factors of pore evolution differ in each period. Continuous distribution of transitional shale gas enrichment areas can be formed along the slope adjacent to coal seams with a moderate maturity range (1.6%–3.0%) in the northeastern Ordos Basin, and transitional shale gas can be enriched in the areas adjacent to coal seams with a moderate maturity range (1.6%–3.0%), abundant fractures, and favorable sealing faults in southwestern Guizhou.

Keywords: Upper Paleozoic; transitional shale gas; lithological associations; gas generation thresholds; pore evolution

1. Introduction

China has conducted considerable research on marine shale of the Lower Cambrian Qiongzhusi and Wufeng-Longmaxi (Upper Ordovician–Lower Silurian) Formations since 2005, and commercial exploitation has been realized to date [1,2]. The first shale gas exploration and evaluation well (W201) obtained industrial gas from marine shale of the Wufeng-Longmaxi Formations (Upper Ordovician–Lower Silurian) in 2010 [3], and then industrial shale gas production was achieved in Fuling, Changning, Weiyuan, and other regions of the Sichuan Basin [4–7]. By the end of 2015, accumulative proven geologic reserves, proven recoverable reserves, and production of shale gas in

China amounted to 5441.29×10^8 m^3, 1360.33×10^8 m^3, and 60×10^8 m^3, respectively, indicating good prospects for rapid development [3]. Scholars have studied marine shale gas enrichment characteristics in China. Guo et al. [8,9] showed that the deep-water shelf shale gas reservoirs of the Wufeng-Longmaxi Formations in the Sichuan Basin are characterized by high total organic carbon content (TOC) and siliceous content levels due to graptolite development, resulting in a high hydrocarbon generation intensity, and reservoirs are easy to fracture and reconstruct. Moreover, tight top and base layers can effectively prevent hydrocarbon from escaping and serve as significant geological factors for shale gas accumulation. Zou et al. [1] deemed that shale gas enrichment and productivity depend on the sedimentary environment, thermal evolution degree, pore and fracture development, and preservation conditions. Jin et al. [10] found that TOC, pore structure, horizontal fractures, high siliceous content, and high formation pressure control the enrichment and high productivity of shale gas. Zhao et al. [11] observed the geological differences between the Lower Cambrian Qiongzhusi and Wufeng-Longmaxi (Upper Ordovician–Lower Silurian) Formations in South China, and concluded that organic-rich intervals development, moderate thermal evolution, rich organic pores, and good top and base layer preservation conditions are the key parameters of shale gas enrichment.

Compared with marine shale, research on Upper Paleozoic transitional shale gas enrichment characteristics in China remains limited. The organic matter (OM) of transitional shale is mainly derived from terrestrial higher plants, and transitional strata are subject to different hydrodynamic forces. Therefore, mudstone is interbedded with sandstone and coal and lithofacies present significant changes in the vertical and horizontal directions in transitional strata, which has important research value. Taking the Lower Permian Shanxi and Pennsylvanian Taiyuan Formations in the northeastern Ordos Basin, and the Upper Permian Longtan Formation in southwestern Guizhou as examples, this research analysed the influence of lithological associations, sedimentary facies, gas generation thresholds, pore evolution, and structural characteristics on Upper Paleozoic transitional shale gas and then studied the shale gas enrichment factors of the northeastern Ordos Basin and southwestern Guizhou.

2. Geological Setting

Two typical areas were selected for study: (1) the Lower Permian Shanxi and Pennsylvanian Taiyuan Formations in the northeastern Ordos Basin, and (2) the Upper Permian Longtan Formation in southwestern Guizhou. The Ordos Basin is characterized by a stable tectonic setting which is not heavily folded or deformed, and Paleozoic-Mesozoic strata in the principal part dip to the west at less than 1° [12–14]. During the late period of the Pennsylvanian, the sedimentary source area in the northern part of the Ordos Basin was uplifted, and delta plain, delta front and tidal flat-lagoon environments predominated from north to south in the northeastern Ordos Basin. During the early period of the Permian, large-scale regressions occurred and the sedimentary source area in the northern part of the Ordos Basin continued uplifting due to hercynian movement, leading to the acceleration of stratigraphic erosion and southward moving rivers, and fluvial, delta plain and front environments formed mainly from north to south in the northeastern Ordos Basin. Southwestern Guizhou experienced long-term tectonic movements which led to the development of folds, faults, and fractures, forming a complex structural morphology [15–17]. Folds are mainly distributed in the northwest direction and anticlines are narrow and steep, while synclines are wide and gentle, forming ejective folds. Faults are mainly distributed in the northeast and northwest directions and show strong heterogeneities. During the late period of the Permian, transgression and regression cycles occurred and the strata was uplifted due to the southward subduction of the Siberia plate. Sedimentary source with a large amount of terrigenous input was deposited in a transitional environment of southwestern Guizhou, forming a delta and a tidal flat-lagoon sedimentary system in the Upper Permian Longtan Formation.

3. Samples and Methods

3.1. Samples

The locations of wells in the northeastern Ordos Basin and southwestern Guizhou are shown in Figures 1A and 2C, respectively. Cores and gas logging data from wells H1 and H2 of the Shanxi and Taiyuan Formations in the northeastern Ordos Basin, and cores and gas desorption data from well X1 of the Longtan Formation in southwestern Guizhou were used to study the relationship between lithological associations and transitional shale gas content. Then, the influence of sedimentary facies on shale gas enrichment was analysed. Samples M1-1, V1-1 and V1-2 from wells M1 (northeastern Ordos Basin) and V1 (southwestern Guizhou) were used for thermal simulation, Rmax measurement, and XRD to study the hydrocarbon generation and clay minerals transformation characteristics during thermal evolution and then the gas generation threshold maturity and pore evolution tendency were determined. Samples from wells M1, M2, L1, L2 and Y1 (northeastern Ordos Basin), and wells V1 and X1 (southwestern Guizhou) were used to study the relationship between Rmax and depth, and the gas generation threshold depths of the northeastern Ordos Basin and southwestern Guizhou were estimated. Combining the structural characteristics of the northeastern Ordos Basin and southwestern Guizhou, Upper Paleozoic transitional shale gas enrichment factors were analysed. Basic data of the samples are shown in Table 1.

Table 1. Basic data of shale samples.

Sample ID	Well	Study Area	Formation	Depth (m)	TOC (wt%)	Kerogen Type	Rmax (%)
M1-1	M1	Northeastern Ordos Basin	Shanxi	1130.4	1.23	III	0.96
M2-1	M2	Northeastern Ordos Basin	Shanxi	1123.1	4.65	III	0.87
L1-1	L1	Northeastern Ordos Basin	Shanxi	2047.0	/	III	1.03
L2-1	L2	Northeastern Ordos Basin	Shanxi	2092.3	/	III	1.07
L2-2	L2	Northeastern Ordos Basin	Taiyuan	2199.8	/	III	1.15
L2-3	L2	Northeastern Ordos Basin	Taiyuan	2222.8	/	III	1.21
Y1-1	Y1	Northeastern Ordos Basin	Shanxi	2397.2	0.97	III	2.63
Y1-2	Y1	Northeastern Ordos Basin	Shanxi	2407.5	1.46	III	2.65
Y1-3	Y1	Northeastern Ordos Basin	Shanxi	2427.2	1.90	III	2.68
Y1-4	Y1	Northeastern Ordos Basin	Shanxi	2455.1	4.62	III	3.20
Y1-5	Y1	Northeastern Ordos Basin	Taiyuan	2497.3	3.06	III	3.30
Y1-6	Y1	Northeastern Ordos Basin	Taiyuan	2501.9	3.21	III	3.32
V1-1	V1	Southwestern Guizhou	Longtan	358.5	5.38	III	0.86
V1-2	V1	Southwestern Guizhou	Longtan	587.0	2.36	III	1.03
V1-3	V1	Southwestern Guizhou	Longtan	678.0	6.53	III	1.06
V1-4	V1	Southwestern Guizhou	Longtan	852.6	2.56	III	1.23
X1-1	X1	Southwestern Guizhou	Longtan	1318.2	2.84	III	2.75
X1-2	X1	Southwestern Guizhou	Longtan	1365.5	5.23	III	2.80
X1-3	X1	Southwestern Guizhou	Longtan	1420.0	3.52	III	2.86

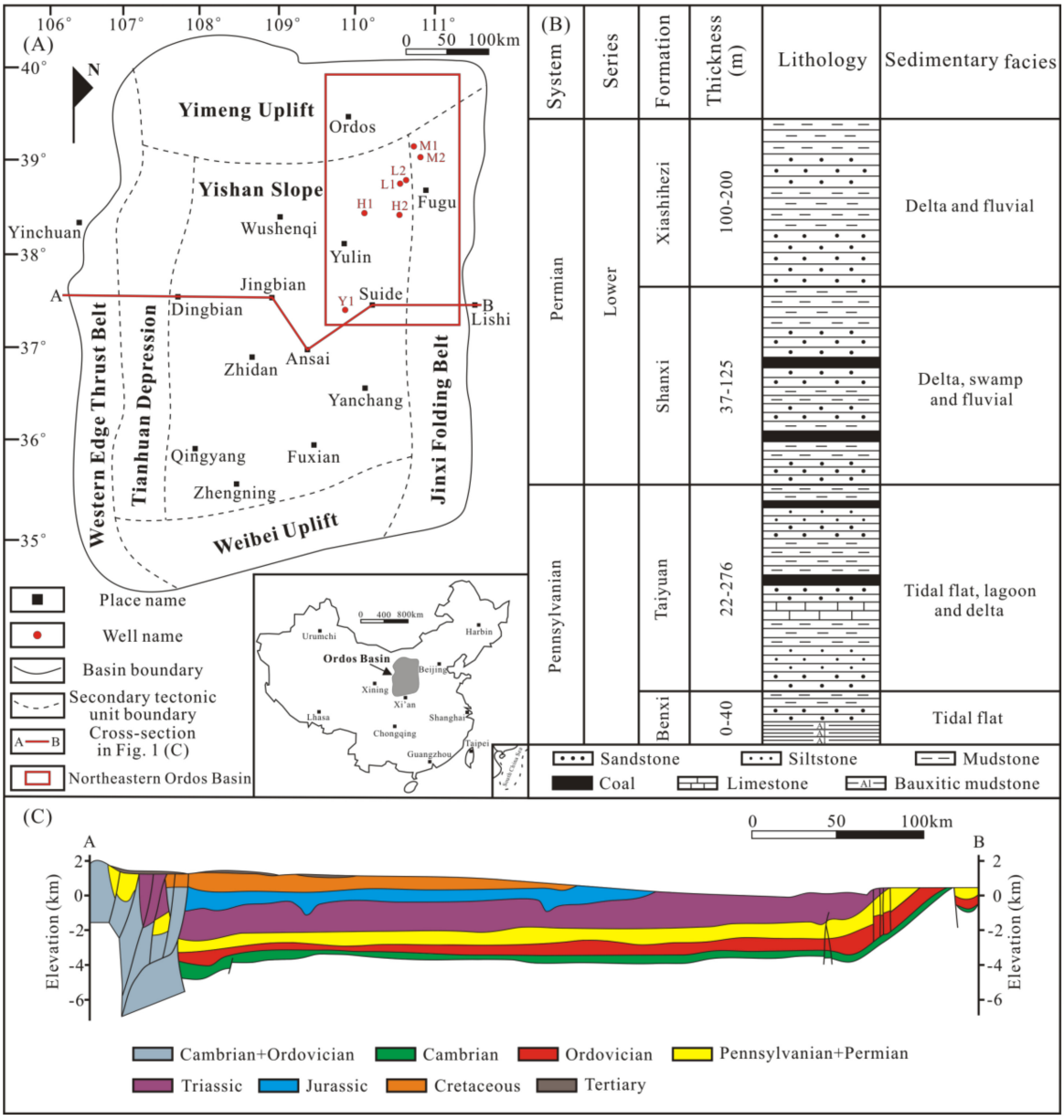

Figure 1. (**A**) Tectonic units and structural cross-section of the Ordos Basin; (**B**) Stratigraphic column and depositional environments of the Pennsylvanian and the Lower Permian strata in the Ordos Basin (modified from Yang et al. [13]; Yang et al. [14]); (**C**) Structural cross-section of the Ordos Basin (modified from Yang et al. [13]).

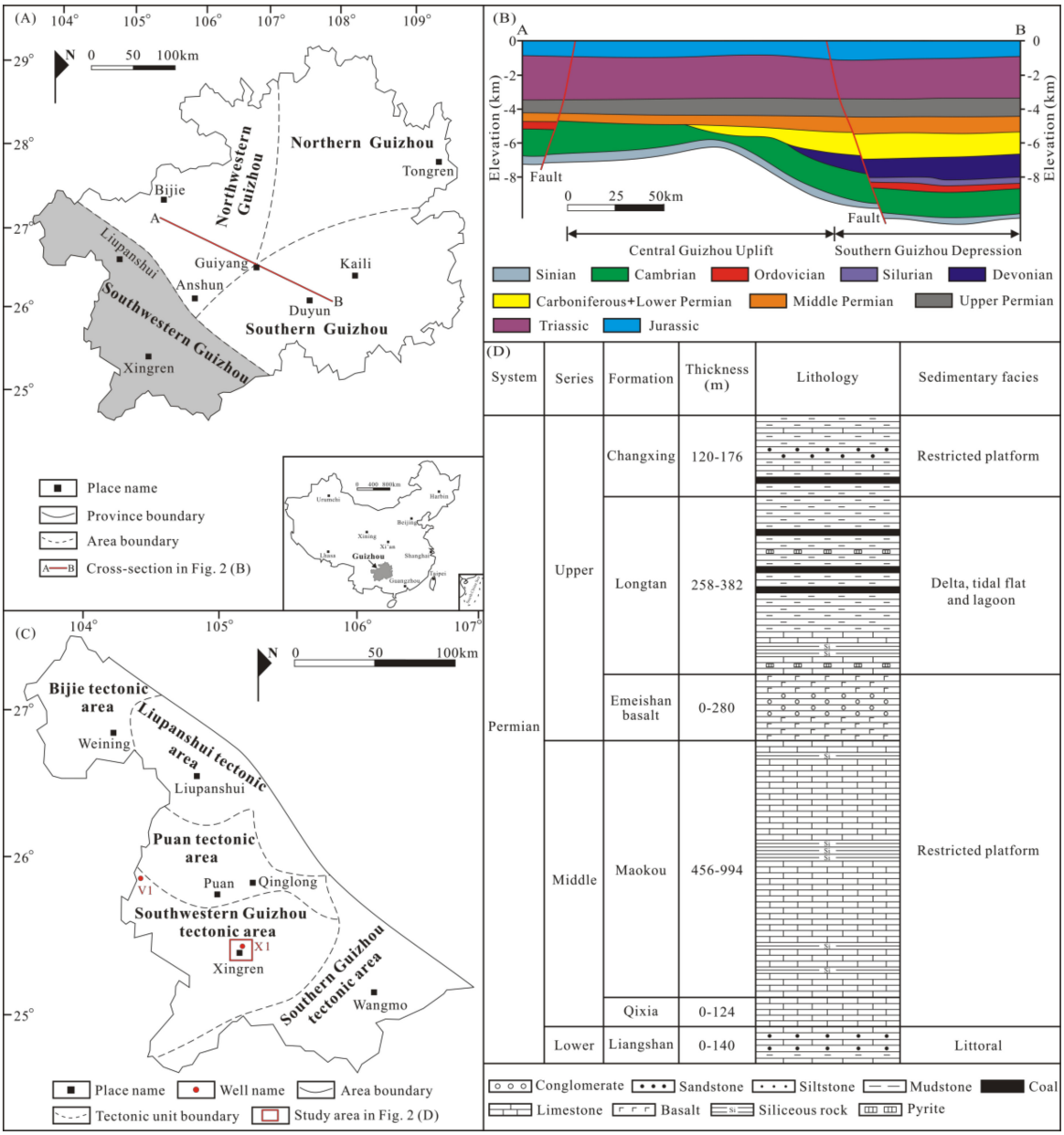

Figure 2. (**A**) Regional division and structural cross-section of Guizhou Province; (**B**) Structural cross-section of Guizhou Province (modified from Luo et al. [18]); (**C**) Tectonic units of southwestern Guizhou; (**D**) Stratigraphic column and depositional environments of the Permian strata in southwestern Guizhou (modified from Ma and Guo [16]).

3.2. *Analytical Methods*

During the gas logging process, drilling fluid was degassed and dried as it circulated to the ground, and hydrocarbon content was measured with a hydrogen flame ionization detector (version, manufacture, city, country) [19–21].

Shale gas desorption was carried out to determine desorbed gas, lost gas, and residual gas contents. A core was placed in closed desorption equipment at the reservoir temperature, and desorbed gas content was measured with a gas metering device, while lost gas content was calculated using the U.S. Bureau of Mines (USBM) method [22]. Then, residual gas content was measured with ground grains of shale sample after desorption. Shale gas content is the sum of desorbed gas, lost gas, and residual gas contents under standard temperature and pressure (STP) conditions (0 °C, 101.325 KPa).

A thermal simulation was conducted to simulate shale maturation through geological time [23–25], and hydrocarbon generation and clay minerals transformation characteristics during thermal evolution were determined. Dried samples were divided into 11 parts, and TOC, kerogen type, and Rmax were measured for 1 part, while thermal simulation was performed on the other 10 parts using a hydrous closed system. Samples for thermal simulation were heated from room temperature to 200–650 °C at intervals of 50 °C with a heating rate of 20 °C/h, respectively [26]. Then, hydrocarbon production (liquid and gaseous hydrocarbons), Rmax, and XRD were obtained with the samples after thermal simulation.

Rmax was used to characterize shale maturity. Kerogens were separated from the shale sample and made into polished sections for measurement using a Zeiss microscope and a TIDAS microspectrophotometer. Fluorescence Alteration of Multiple Macerals (FAMM) technology was used for the correction of reflectance [27]. The polished section on the stage was rotated for 360° slowly and then Rmax was determined based on the principle of photoelectric effect.

XRD was used to calculate the relative contents of minerals. The samples were ground into powders of 325–400 mesh sizes and performed with an X-ray diffractometer. Then, the mineral percentages were estimated semi-quantitatively by the area under the curve for the major peak with correction for Lorentz Polarization.

4. Results and Discussion

4.1. Lithological Associations and Sedimentary Facies

Transitional strata natural gas mainly includes shale gas, coal bed methane (CBM), and sandstone gas. Shale gas occurs mainly as adsorbed and free gas [28–30], and CBM occurs mainly in the adsorption state [31,32], while sandstone gas occurs mainly in the free state and reservoir space and cap rock control gas accumulation [33]. As three types of gas reservoirs are superposed onto each other in the vertical and horizontal directions within transitional strata, lithological associations have an important influence on shale gas enrichment characteristics. According to the cores and gas logging data from wells H1 and H2 of the Shanxi and Taiyuan Formations in the northeastern Ordos Basin (Figures 3 and 4), and the cores and gas desorption data from well X1 of the Longtan Formation in southwestern Guizhou (Figure 5), carbonaceous mudstone adjacent to coal seams presents a high gas content level. Carbonaceous mudstone is rich in OM and has a strong gaseous hydrocarbon generation capacity. In addition, the migration of CBM to adjacent shale can increase the shale gas content levels. Together, these characteristics result in shale gas enrichment. Carbonaceous mudstone adjacent to coal seams is primarily developed in swamps in the delta plain environment, and lagoons and swamps in the barrier coastal environment (Figures 3–5).

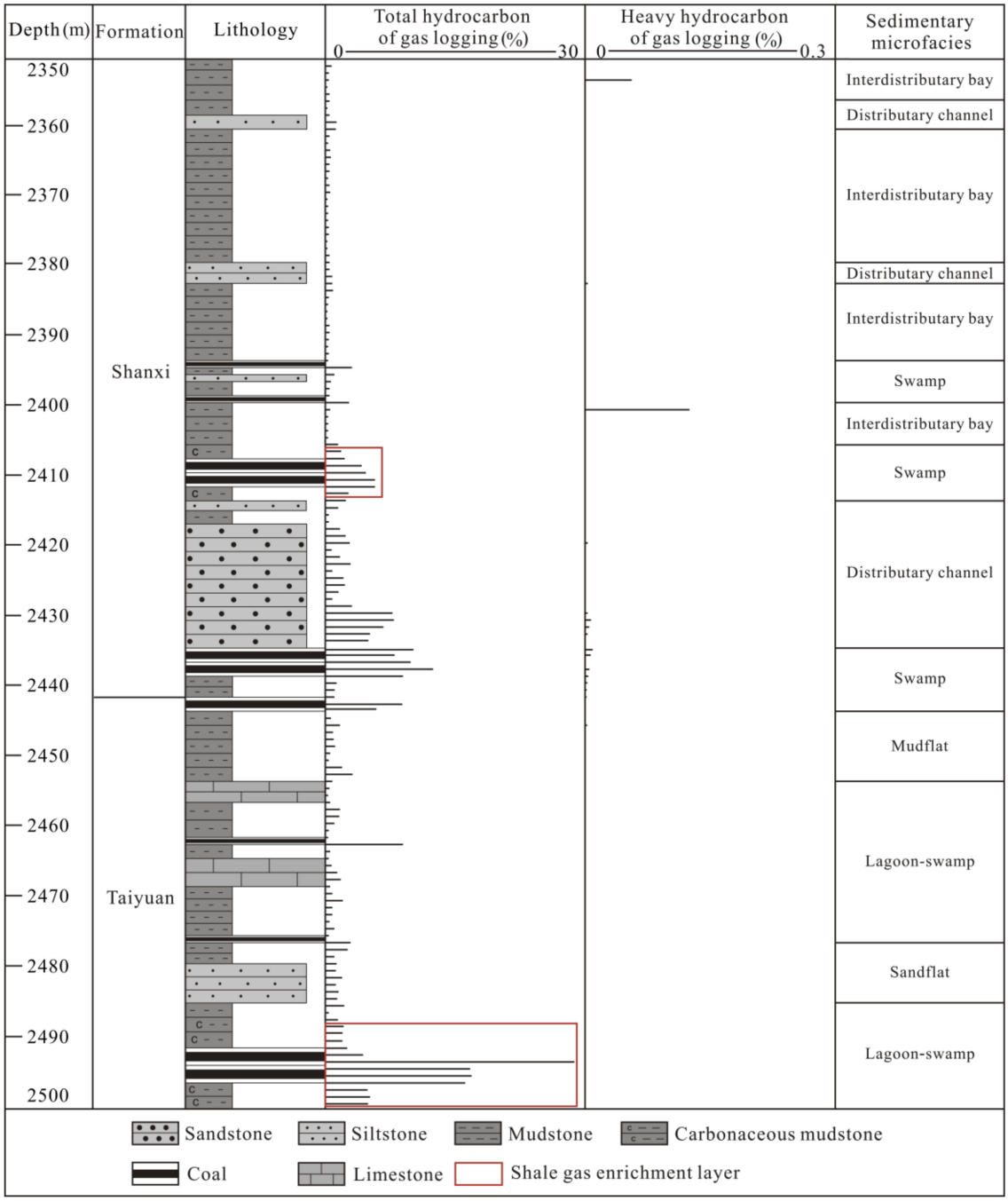

Figure 3. Stratigraphic column, gas logging and depositional environments of the Lower Permian Shanxi and Pennsylvanian Taiyuan Formations in Well H1, northeastern Ordos Basin.

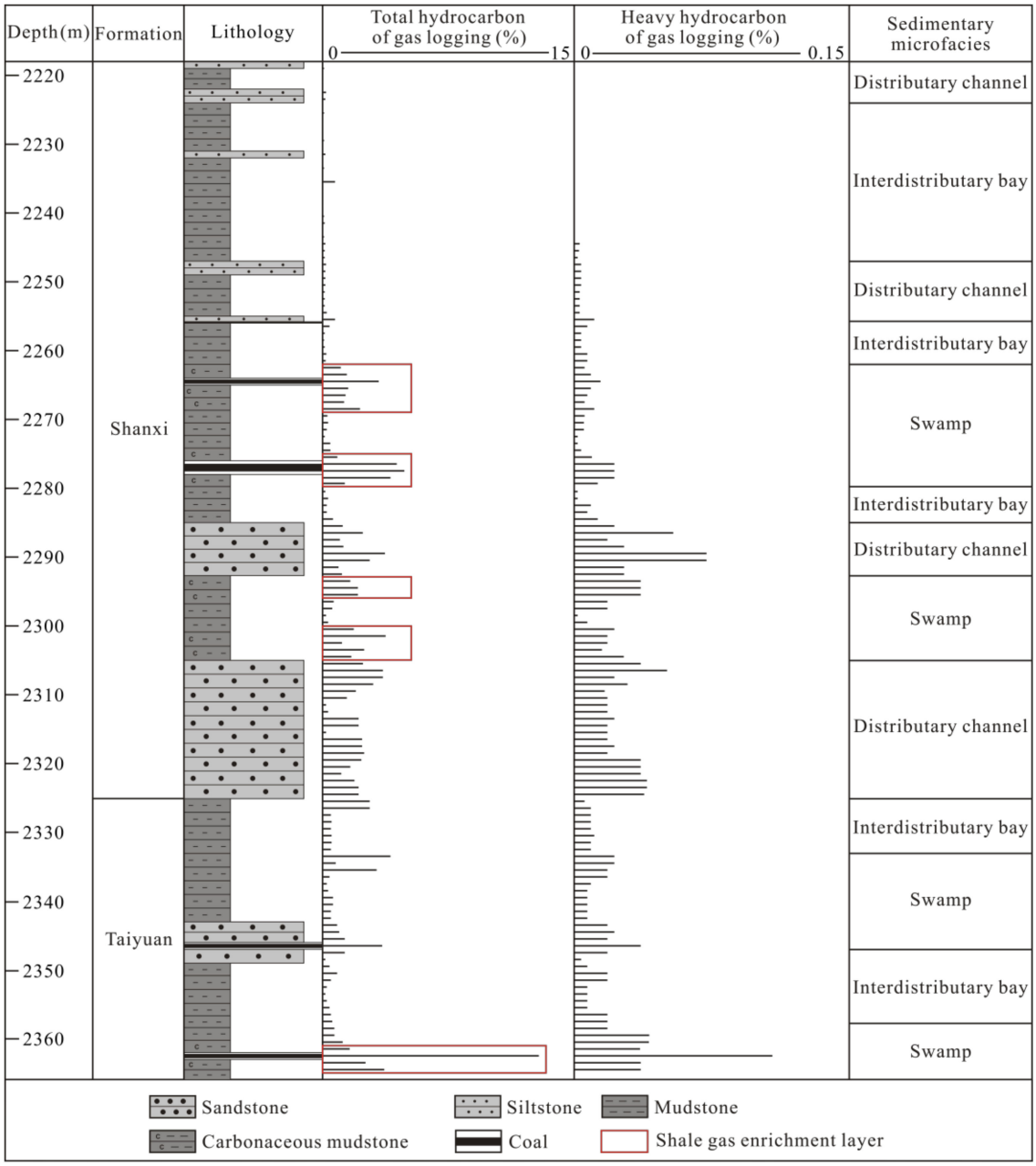

Figure 4. Stratigraphic column, gas logging and depositional environments of the Lower Permian Shanxi and Pennsylvanian Taiyuan Formations in Well H2, northeastern Ordos Basin.

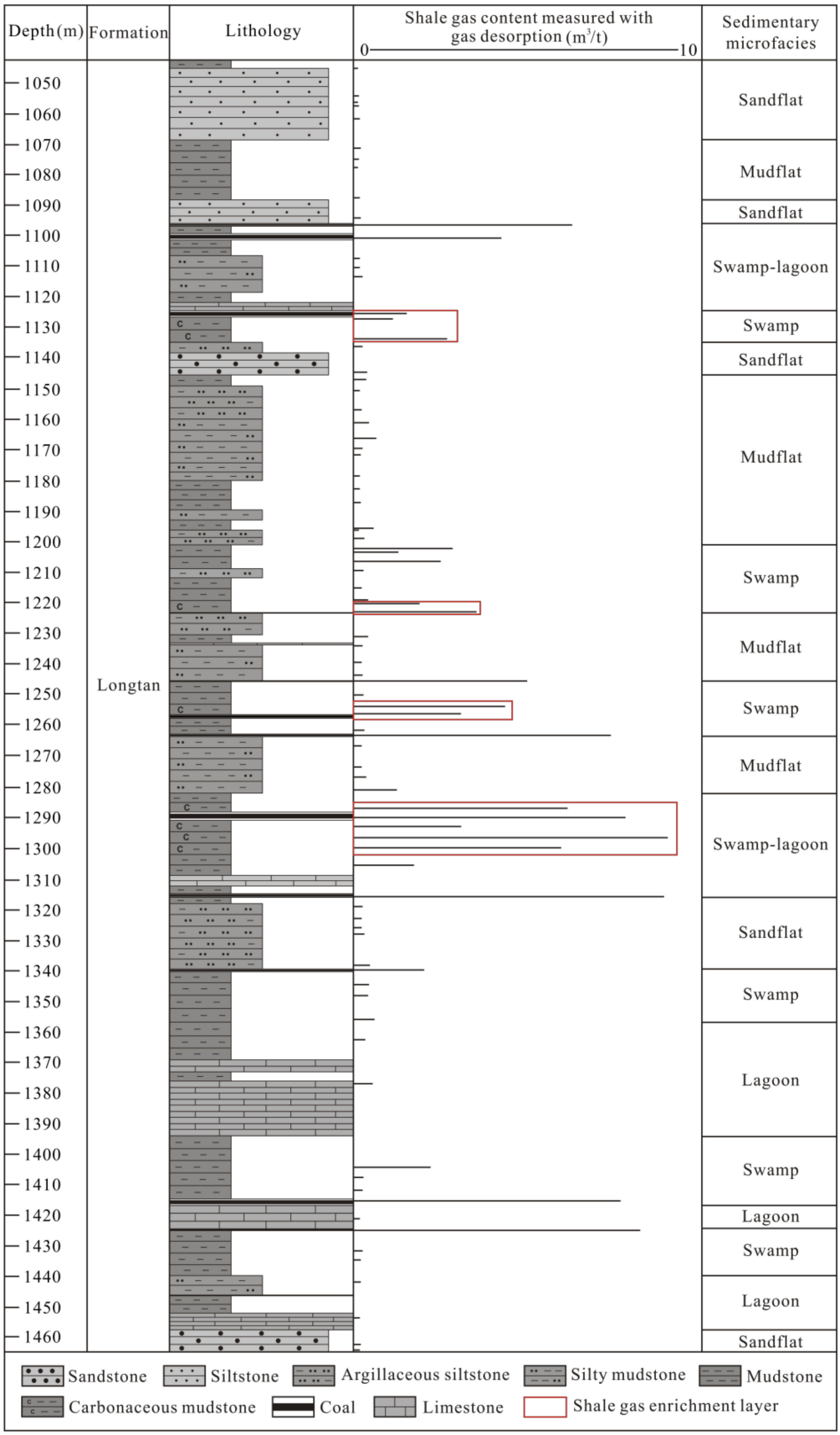

Figure 5. Stratigraphic column, gas desorption and depositional environments of the Upper Permian Longtan Formation in Well X1, southwestern Guizhou.

A delta forms at the interface of marine and continental environments and is related to river channel and overbank settings and occurs alongside wave and tidal action of the shallow marine realm. It consists of the delta plain, delta front, and prodelta [34]. The swamp is mainly distributed in the delta plain, which is a low-lying area that is periodically submerged in water and in a reducing environment. The lithologies mainly include carbonaceous mudstone and coal, and massive and horizontal beddings are developed. The swamp is characterized by warm and humid climatic environments and abundant plants [35], leading to the enrichment of OM and mudstone interbedded with coal (Figure 6).

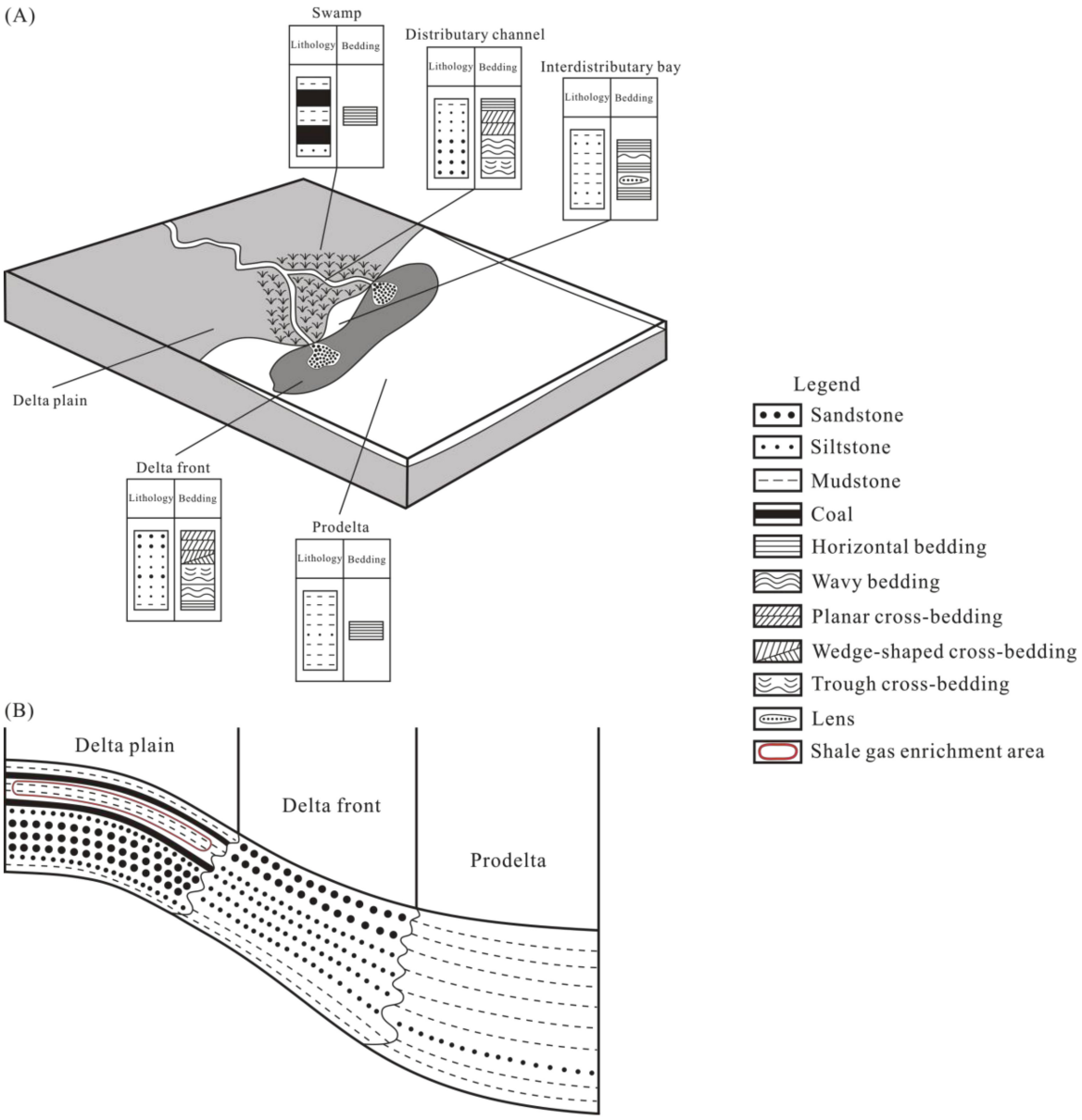

Figure 6. Shale gas enrichment characteristics of a delta environment: (**A**) stereogram (modified from Nichols [34]); (**B**) profile.

The barrier coast is developed in a transitional environment within which barrier island-tidal flat-lagoon-swamp systems can be formed [34]. The lagoon is a coastal body with very limited connections to the open ocean. The sediments are mainly fine-grained, and horizontal bedding is developed. The lagoon is in a quiet and low-energy environment in which large quantities of sediments are carried by rivers under rainy weather conditions. Anaerobic bacteria reproduce in the lower part of lagoon to form a reducing environment [36], which is favorable to the preservation of OM, forming

an organic-rich shale and shale gas enrichment area (Figure 7). The swamp is widely distributed in the supralittoral zone, which presents a relatively weak hydrodynamic environment and fine-grained sediments. Abundant plants in the swamp lead to OM enrichment, and frequent alternations of high and low water levels result in mudstone interbedded with coal (Figure 7).

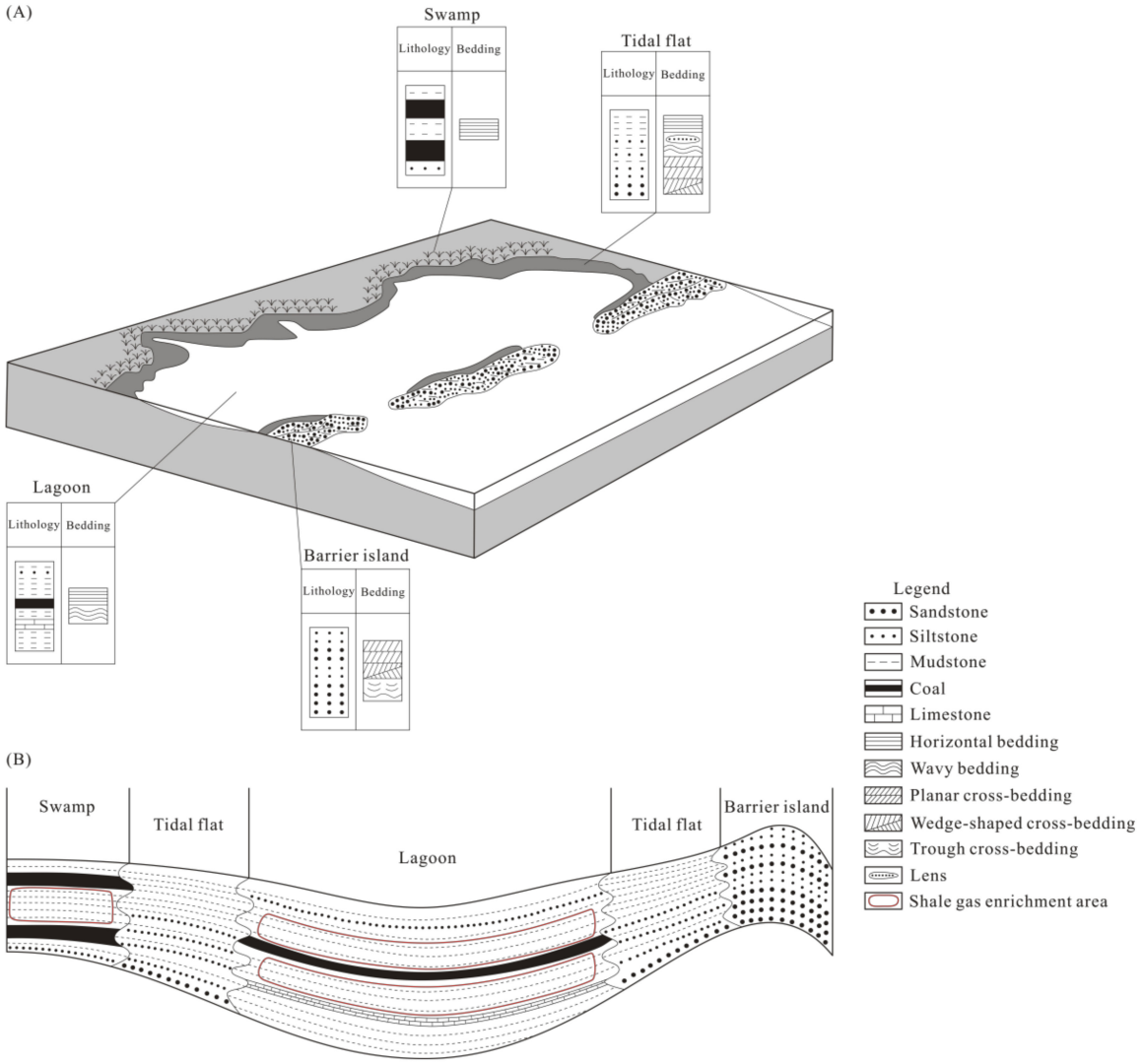

Figure 7. Shale gas enrichment characteristics of a barrier coastal environment: (**A**) stereogram (modified from Nichols [34]); (**B**) profile.

4.2. Gas Generation Thresholds

Hydrocarbon generation contents (liquid and gaseous hydrocarbons) during thermal evolution were determined by thermal simulation, hydrocarbon production and Rmax measurements using samples M1-1, V1-1, and V1-2 (Table 1). Hydrocarbon generation contents increase with increasing Rmax values during thermal evolution, while liquid hydrocarbon contents first increase when Rmax < 1.6% and then decrease and gaseous hydrocarbon contents begin to increase rapidly when Rmax > 1.6% due to kerogen pyrolysis and liquid hydrocarbon cracking. Therefore, the gas generation threshold maturity (Rmax) of transitional shale is 1.6%. Previous studies indicated that relations between vitrinite reflectance and depth show upper and lower segments, and the reflectance in the lower segment increases more rapidly than in the upper segment [37,38]. Therefore, the variation tendency of Rmax with depth was established with the Rmax values and depths of the Shanxi and Taiyuan Formations in the northeastern Ordos Basin and Longtan Formation in southwestern Guizhou,

and then the corresponding threshold depths of the northeastern Ordos Basin (about 2265 m) and southwestern Guizhou (about 1050 m) were estimated. Relationship between Rmax and depth is shown in Figure 8, while hydrocarbon generation characteristic and gas generation thresholds of transitional shale are shown in Figure 9.

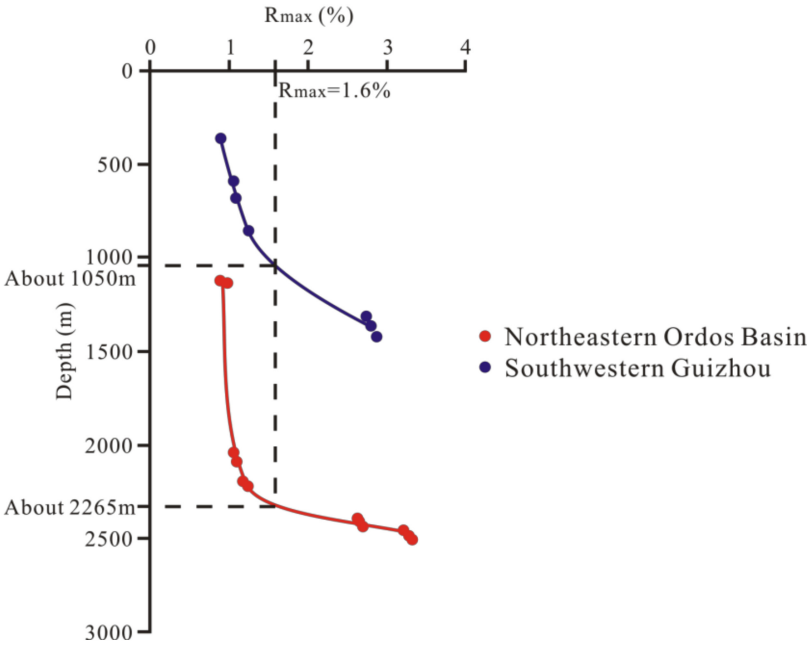

Figure 8. Relationship between Rmax and depth of the Shanxi and Taiyuan Formations in the northeastern Ordos Basin and Longtan Formation in southwestern Guizhou.

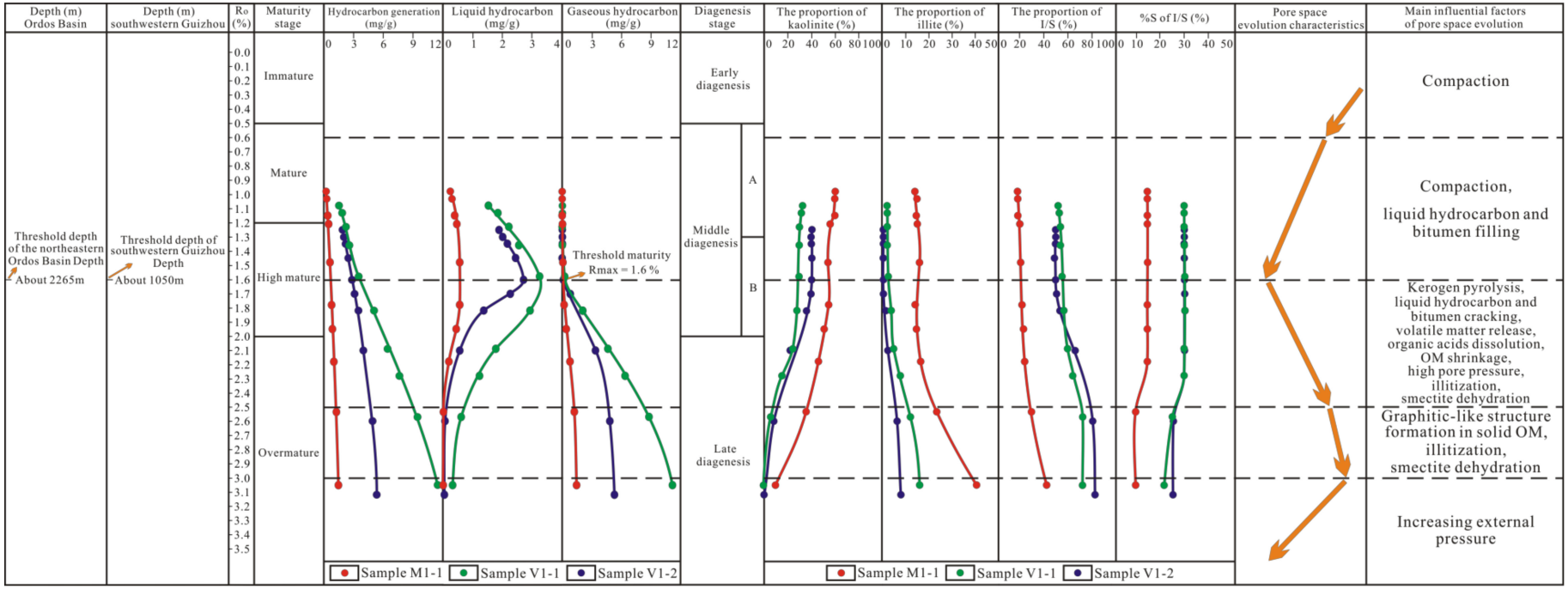

Figure 9. Hydrocarbon generation, clay minerals transformation, and pore evolution characteristics based on thermal simulation.

4.3. Pore Evolution

Pores are the main reservoir space of shale and can be classified into micropores (<2 nm), mesopores (2–50 nm), and macropores (>50 nm) based on the International Union of Pure and Applied Chemistry (IUPAC) classification criteria [39]. Pore evolution through geological time is jointly controlled by hydrocarbon generation [40,41], clay minerals transformation [42,43], and compaction [44–46]. Thermal simulation, hydrocarbon production, Rmax measurement, and XRD were used to study transitional shale maturation, hydrocarbon generation, and clay minerals transformation characteristics during thermal evolution (Figure 9). Maturity was divided into the immature stage (R_o < 0.5%), the mature stage (0.5% < R_o < 1.2%), the high mature stage (1.2% < R_o < 2.0%), and the overmature stage (R_o > 2.0%) according to Liu and Zhang [47], and diagenesis was divided into the early diagenesis stage (R_o < 0.5%), the middle diagenesis A stage (0.5% < R_o < 1.3%), the middle diagenesis B stage (1.3% < R_o < 2.0%), and the late diagenesis stage (R_o > 2.0%) according to the Chinese Oil and Gas Industry Standard SY/T 5477 [48].

When Rmax < 0.6%, transitional shale is in the submature stage, while hydrocarbon generation and clay minerals transformation are not obvious. Compaction is the main factor decreasing pore space [44,46], and macropores are more easy to compact than micropores and mesopores [45].

When 0.6% < Rmax < 1.6%, transitional shale enters the "oil window" [49,50] and kerogen pyrolysis generates a large number of liquid hydrocarbons, but few gaseous hydrocarbons are generated. Moreover, clay minerals transformation is not obvious, indicating that the transformation occurs mainly in the middle diagenesis B and late diagenesis stages. Micropores and mesopores are infilled by liquid hydrocarbon and bitumen due to large surface areas [51,52] and macropores are compacted during the period, leading to a decrease in the pore space.

When 1.6% < Rmax < 2.5%, transitional shale enters gas generation threshold. Gaseous hydrocarbon content begins to increase rapidly due to kerogen pyrolysis and cracking of liquid hydrocarbon and bitumen, while liquid hydrocarbon content reaches its maximum value and then decreases. Kaolinite begins to convert to illite rapidly and generate illite/smectite (I/S) as an intermediate product [53], leading to the decrease in kaolinite and increase in illite and I/S, while smectite in I/S converts to illite during the period. Kerogen pyrolysis, liquid hydrocarbon and bitumen cracking, and volatile matter release generate nearly circular or bubble-like pores in OM [54,55] and gaseous hydrocarbon generation forms high pore pressure resisting further compaction [56,57], while OM shrinkage forms fissures [58]. Organic acids originating from kerogen decarboxylation, hydrocarbon cracking, and minerals oxidation dissolve feldspar and clay mineral to form secondary pores [59,60]. Illitization of kaolinite dissolves feldspar [61,62], while the Fe^{3+} from the conversion of smectite to illite in I/S promotes the release of the peripheral dicarboxylic acid group from kerogen and improves the formation of carboxylic acids and phenols [63], which contribute to the development of secondary dissolved pores. Moreover, the smectite dehydration enhances the formation of fissures [64,65]. Together, these processes increase pore space.

When 2.5% < Rmax < 3.0%, transitional shale hydrocarbon generation tends to the end, while clay minerals transformation is still proceeding rapidly. During this period, the increase in pore space is jointly controlled by a graphitic-like structure with abundant nanopores which is generated in solid OM [54], illitization of kaolinite which dissolves feldspar [61,62], and smectite dehydration which forms shrinkage cracks [64,65].

When Rmax > 3.0%, transitional shale hydrocarbon generation and clay minerals transformation come to the end. Increasing external pressure leads to pore collapse [44,57] and decreases pore space.

Therefore, transitional shale pore space may have the tendency to decrease when Rmax < 1.6% or Rmax > 3.0% but increase when Rmax ranges between 1.6% and 3.0%. The main influential factors of pore evolution differ in each period.

According to the transitional shale gas generation threshold maturity (Rmax = 1.6%) and pore evolution tendency (increase when Rmax ranges between 1.6% and 3.0%), shale gas exploration should focus on the areas with a maturity range of 1.6%–3.0%.

4.4. Upper Paleozoic Transitional Shale Gas Enrichment Factors

Taking the Lower Permian Shanxi and Pennsylvanian Taiyuan Formations in the northeastern Ordos Basin, and the Upper Permian Longtan Formation in southwestern Guizhou as examples, Upper Paleozoic transitional shale gas enrichment factors were analysed. Lithological associations, sedimentary facies, gas generation threshold, pore space, and structural characteristics are the main controlling factors of Upper Paleozoic transitional shale gas enrichment. As discussed in Section 4.1, Section 4.2, Section 4.3, carbonaceous mudstone adjacent to coal seams, which is primarily developed in swamps in the delta plain environment, and lagoons and swamps in the barrier coastal environment, presents a high gas content level. The gas generation threshold maturity (Rmax) is 1.6%, and pore space has the tendency to increase when Rmax ranges between 1.6% and 3.0%, so shale gas is mainly distributed in the areas with a maturity range of 1.6%–3.0%. Upper Paleozoic strata of the northeastern Ordos Basin and southwestern Guizhou present different structural characteristics. The Ordos Basin is a stable multicycle cratonic basin which is not heavily folded or deformed, and Paleozoic-Mesozoic strata in the main section dip to the west at less than 1° [12,13], which leads to the continuous distribution of shale gas enrichment areas along the slope (Figure 10). Long-term tectonic movements lead to the development of folds, faults, and fractures, forming a complex structural morphology [15–17]. Fractures enrich the reservoir space, favoring shale gas storage and reservoir reconstruction, and sealing faults can prevent shale gas migration to adjacent formation. Therefore, shale gas can be enriched in the areas with abundant fractures and favorable sealing faults in southwestern Guizhou (Figure 11).

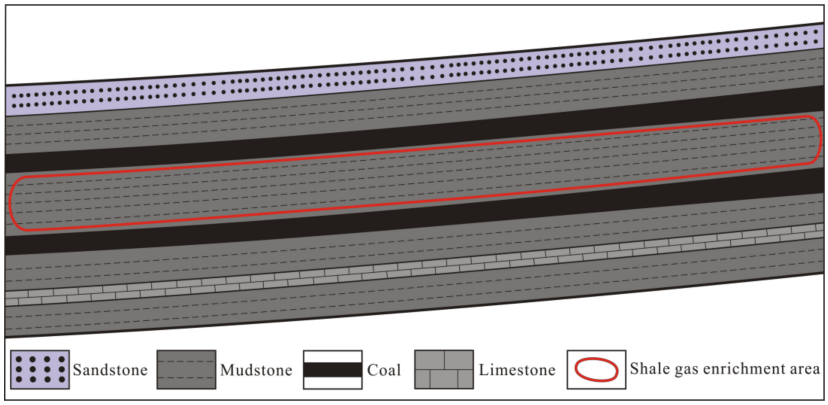

Figure 10. Shale gas enrichment characteristics of the Shanxi and Taiyuan Formations in the northeastern Ordos Basin.

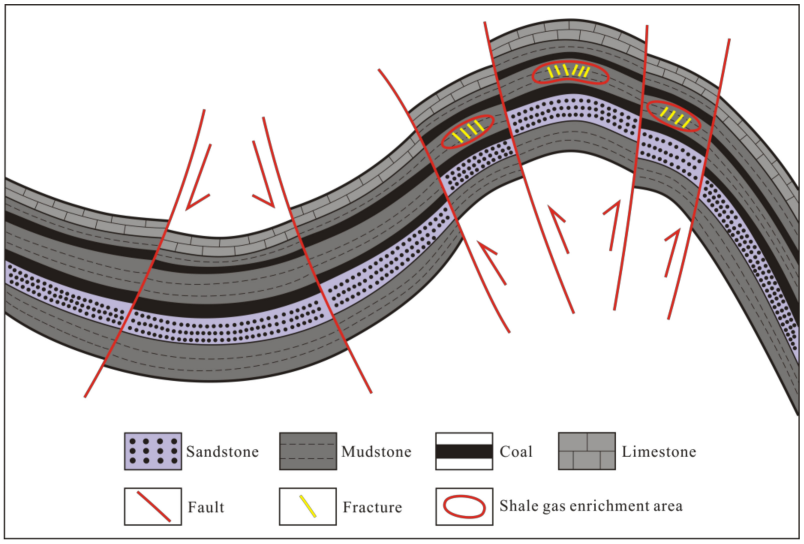

Figure 11. Shale gas enrichment characteristics of the Longtan Formation in southwestern Guizhou.

5. Conclusions

1. Gas logging and desorption revealed carbonaceous mudstone adjacent to coal seams presents a high gas content level due to abundant OM and gas migration from coal seams, and is primarily developed in swamps in the delta plain environment, and swamps and lagoons in the barrier coastal environment.
2. Gas generation threshold maturity (Rmax) of transitional shale is 1.6%, and corresponding threshold depths of the northeastern Ordos Basin and southwestern Guizhou are about 2265 m and 1050 m.
3. Transitional shale pore evolution is jointly controlled by hydrocarbon generation, clay minerals transformation, and compaction. When Rmax < 1.6%, pore space may decrease due to compaction and filling of liquid hydrocarbon and bitumen. When Rmax ranges between 1.6% and 3.0%, pore space may increase due to kerogen pyrolysis, liquid hydrocarbon and bitumen cracking, volatile matter release, organic acids dissolution, OM shrinkage, high pore pressure, graphitic-like structure formation in solid OM, illitization, and smectite dehydration. When Rmax > 3.0%, transitional shale pore space may decrease due to increasing external pressure.
4. The continuous distribution of transitional shale gas enrichment areas can be formed along the slope adjacent to coal seams with a moderate maturity range (1.6%–3.0%) in the northeastern Ordos Basin, while transitional shale gas can be enriched in the areas adjacent to coal seams with a moderate maturity range (1.6%–3.0%), abundant fractures, and favorable sealing faults in southwestern Guizhou.

Author Contributions: F.W. conceived the research plan, analysed the research data, designed the figures, and wrote the original manuscript. S.G. designed the experiment and was responsible for the project administration, supervision and validation. All authors participated in writing and revising the manuscript. All authors have read and agreed to the published version of the manuscript.

Funding: The research was financially supported by the National Major Science and Technology Project: Study on the Upper Paleozoic transitional shale gas occurrence and enrichment mechanisms (2016ZX05034001-004).

Acknowledgments: We would like to thank the help of the Oil & Gas Survey, China Geological Survey for the study.

Conflicts of Interest: The authors declare no conflict of interest.

References

1. Zou, C.; Dong, D.; Wang, Y.; Li, X.; Huang, J.; Wang, S.; Guan, Q.; Zhang, C.; Wang, H.; Liu, H.; et al. Shale gas in China: Characteristics, challenges and prospects (I). *Pet. Explor. Dev.* **2015**, *42*, 753–767. [CrossRef]
2. Zou, C.; Dong, D.; Wang, Y.; Li, X.; Huang, J.; Wang, S.; Guan, Q.; Zhang, C.; Wang, H.; Liu, H.; et al. Shale gas in China: Characteristics, challenges and prospects (II). *Pet. Explor. Dev.* **2016**, *43*, 182–196. [CrossRef]
3. Dong, D.; Wang, Y.; Li, X.; Zou, C.; Guan, Q.; Zhang, C.; Huang, J.; Wang, S.; Wang, H.; Liu, H.; et al. Breakthrough and prospect of shale gas exploration and development in China. *Nat. Gas Ind.* **2016**, *3*, 12–26. [CrossRef]
4. Li, H.; Tang, H.; Zheng, M. Micropore Structural Heterogeneity of Siliceous Shale Reservoir of the Longmaxi Formation in the Southern Sichuan Basin, China. *Minerals* **2019**, *9*, 548. [CrossRef]
5. Yang, F.; Ning, Z.; Wang, Q.; Zhang, R.; Krooss, B.M. Pore structure characteristics of lower Silurian shales in the southern Sichuan Basin, China: Insights to pore development and gas storage mechanism. *Int. J. Coal Geol.* **2016**, *156*, 12–24. [CrossRef]
6. Liang, H.; Xu, F.; Xu, G.; Yuan, H.; Huang, S.; Wang, Y.; Wang, L.; Fu, D. Geochemical characteristics and origins of the diagenetic fluids of the Permian Changxing Formation calcites in the Southeastern Sichuan Basin: Evidence from petrography, inclusions and Sr, C and O isotopes. *Mar. Pet. Geol.* **2019**, *103*, 564–580. [CrossRef]
7. Xu, H.; Zhou, W.; Zhang, R.; Liu, S.; Zhou, Q. Characterizations of pore, mineral and petrographic properties of marine shale using multiple techniques and their implications on gas storage capability for Sichuan Longmaxi gas shale field in China. *Fuel* **2019**, *241*, 360–371. [CrossRef]

8. Guo, X. Rules of two-factor enrichment for marine shale gas in southern China: Understanding from the Longmaxi Formation shale gas in Sichuan Basin and its surrounding area. *Acta Geol. Sin.* **2014**, *88*, 1209–1218, (In Chinese with English abstract).
9. Guo, X.; Hu, D.; Li, Y.; Wei, X.; Liu, Z. Geological factors controlling shale gas enrichment and high production in Fuling shale gas field. *Pet. Explor. Dev.* **2017**, *44*, 513–523. [CrossRef]
10. Jin, Z.; Hu, Z.; Gao, B.; Zhao, J. Controlling factors on the enrichment and high productivity of shale gas in the Wufeng-Longmaxi Formations, southeastern Sichuan Basin. *Earth Sci. Front.* **2016**, *23*, 1–10, (In Chinese with English abstract).
11. Zhao, W.; Li, J.; Yang, T.; Wang, S.; Huang, J. Geological difference and its significance of marine shale gases in South China. *Pet. Explor. Dev.* **2016**, *43*, 547–559. [CrossRef]
12. He, C.; Ji, L.; Wu, Y.; Su, A.; Zhang, M. Characteristics of hydrothermal sedimentation process in the Yanchang Formation, south Ordos Basin, China: Evidence from element geochemistry. *Sediment. Geol.* **2016**, *345*, 33–41. [CrossRef]
13. Yang, Y.; Li, W.; Ma, L. Tectonic and stratigraphic controls of hydrocarbon systems in the Ordos basin: A multicycle cratonic basin in central China. *AAPG Bull.* **2005**, *89*, 255–269. [CrossRef]
14. Yang, H.; Fu, J.; Wei, X.; Liu, X. Sulige field in the Ordos Basin: Geological setting, field discovery and tight gas reservoirs. *Mar. Pet. Geol.* **2008**, *25*, 387–400. [CrossRef]
15. Dai, S.; Ren, D.; Hou, X.; Shao, L. Geochemical and mineralogical anomalies of the late Permian coal in the Zhijin coalfield of southwest China and their volcanic origin. *Int. J. Coal Geol.* **2003**, *55*, 117–138. [CrossRef]
16. Ma, X.; Guo, S. Comparative Study on shale characteristics of different sedimentary microfacies of Late Permian Longtan Formation in Southwestern Guizhou, China. *Minerals* **2019**, *9*, 20. [CrossRef]
17. Xie, P.; Hower, J.C.; Liu, X. Petrographic characteristics of the brecciated coals from Panxian county, Guizhou, southwestern China. *Fuel* **2019**, *243*, 1–9. [CrossRef]
18. Luo, W.; Hou, M.; Liu, X.; Huang, S.; Chao, H.; Zhang, R.; Deng, X. Geological and geochemical characteristics of marine-continental transitional shale from the Upper Permian Longtan formation, Northwestern Guizhou, China. *Mar. Pet. Geol.* **2018**, *89*, 58–67. [CrossRef]
19. Erzinger, J.; Wiersberg, T.; Dahms, E. Real-time mud gas logging during drilling of the SAFOD Pilot Hole in Parkfield, CA. *Geophys. Res. Lett.* **2004**, 31. [CrossRef]
20. Erzinger, J.; Wiersberg, T.; Zimmer, M. Real-time mud gas logging and sampling during drilling. *Geofluids* **2006**, *6*, 225–233. [CrossRef]
21. McKinney, D.E.; Flannery, M.; Elshahawi, H.; Stankiewicz, A.; Clarke, E.; Breviere, J.; Sachin, S. Advanced mud gas logging in combination with wireline formation testing and geochemical fingerprinting for an improved understanding of reservoir architecture. In *SPE Annual Technical Conference and Exhibition*; Society of Petroleum Engineers: Anaheim, CA, USA, 2007.
22. Diamond, W.P.; Levine, J.R. Direct method determination of the gas content of coal: Procedures and results. In *Bureau of Mines Report of Investigations*; US Department of the Interior, Bureau of Mines: Washington, DC, USA, 1981.
23. Lewan, M.D.; Bjorøy, M.; Dolcater, D.L. Effects of thermal maturation on steroid hydrocarbons as determined by hydrous pyrolysis of Phosphoria Retort Shale. *Geochim. Cosmochim. Acta* **1986**, *50*, 1977–1987. [CrossRef]
24. Hu, H.; Zhang, T.; Wiggins-Camacho, J.; Ellis, G.; Lewan, M.; Zhang, X. Experimental investigation of changes in methane adsorption of bitumen-free Woodford Shale with thermal maturation induced by hydrous pyrolysis. *Mar. Pet. Geol.* **2015**, *59*, 114–128. [CrossRef]
25. Spigolon, A.L.; Lewan, M.D.; de Barros Penteado, H.L.; Coutinho, L.F.C.; Mendonça Filho, J.G. Evaluation of the petroleum composition and quality with increasing thermal maturity as simulated by hydrous pyrolysis: A case study using a Brazilian source rock with Type I kerogen. *Org. Geochem.* **2015**, *83*, 27–53. [CrossRef]
26. Wang, F.; Guo, S. Shale gas content evolution in the Ordos Basin. *Int. J. Coal Geol.* **2019**, *211*, 103231. [CrossRef]
27. Lo, H.B.; Wilkins, R.W.T.; Ellacott, M.V.; Buckingham, C.P. Assessing the maturity of coals and other rocks from north america using the fluorescence alteration of multiple macerals (FAMM) technique. *Int. J. Coal Geol.* **1997**, *33*, 61–71. [CrossRef]
28. Jarvie, D.M.; Hill, R.J.; Ruble, T.E.; Pollastro, R.M. Unconventional shale-gas systems: The Mississippian Barnett Shale of north-central Texas as one model for thermogenic shale-gas assessment. *AAPG Bull.* **2007**, *91*, 475–499. [CrossRef]

29. Ross, D.J.K.; Bustin, R.M. Characterizing the shale gas resource potential of Devonian-Mississippian strata in the Western Canada sedimentary basin: Application of an integrated formation evaluation. *AAPG Bull.* **2008**, *92*, 87–125. [CrossRef]
30. Tang, L.; Song, Y.; Jiang, Z.; Pang, X.; Li, Z.; Li, Q.; Li, W.; Tang, X.; Pan, A. Influencing factors and mathematical prediction of shale adsorbed gas content in the Upper Triassic Yanchang Formation in the Ordos Basin, China. *Minerals* **2019**, *9*, 625. [CrossRef]
31. Bustin, R.M.; Clarkson, C.R. Geological controls on coalbed methane reservoir capacity and gas content. *Int. J. Coal Geol.* **1998**, *38*, 3–26. [CrossRef]
32. Meng, Z.; Yan, J.; Li, G. Controls on gas content and carbon isotopic abundance of methane in Qinnan-East coal bed methane block, Qinshui Basin, China. *Energy Fuels* **2017**, *31*, 1502–1511. [CrossRef]
33. Zou, C.; Zhu, R.; Liu, K.; Su, L.; Bai, B.; Zhang, X.; Yuan, X.; Wang, J. Tight gas sandstone reservoirs in China: Characteristics and recognition criteria. *J. Pet. Sci. Eng.* **2012**, *88*, 82–91. [CrossRef]
34. Nichols, G. *Sedimentology and Stratigraphy*, 2nd ed.; John Wiley & Sons: Hoboken, NJ, USA, 2009.
35. Jasper, K.; Hartkopf-Fröder, C.; Flajs, G.; Littke, R. Evolution of Pennsylvanian (Late Carboniferous) peat swamps of the Ruhr Basin, Germany: Comparison of palynological, coal petrographical and organic geochemical data. *Int. J. Coal Geol.* **2010**, *83*, 346–365. [CrossRef]
36. McLaughlin, M.R.; Brooks, J.P.; Adeli, A. Characterization of selected nutrients and bacteria from anaerobic swine manure lagoons on sow, nursery, and finisher farms in the Mid-South USA. *J. Environ. Qual.* **2009**, *38*, 2422–2430. [CrossRef] [PubMed]
37. Suggate, R.P. Relations between depth of burial, vitrinite reflectance and geothermal gradient. *J. Pet. Geol.* **1998**, *21*, 5–32. [CrossRef]
38. Law, B.E.; Nuccio, V.F.; Barker, C.E. Kinky vitrinite reflectance well profiles: Evidence of paleopore pressure in low-permeability, gas-bearing sequences in Rocky Mountain foreland basins. *AAPG Bull.* **1989**, *73*, 999–1010.
39. International Union of Pure and Applied Chemistry. Physical chemistry division commission on colloid and surface chemistry, subcommittee on characterization of porous solids: Recommendations for the characterization of porous solids. (Technical Report). *Pure Appl. Chem.* **1994**, *66*, 1739–1758. [CrossRef]
40. Hill, R.J.; Zhang, E.; Katz, B.J.; Tang, Y. Modeling of gas generation from the Barnett shale, Fort Worth Basin, Texas. *AAPG Bull.* **2007**, *91*, 501–521. [CrossRef]
41. Lu, J.; Ruppel, S.C.; Rowe, H.D. Organic matter pores and oil generation in the Tuscaloosa marine shale. *AAPG Bull.* **2015**, *99*, 333–357. [CrossRef]
42. Chalmers, G.R.; Bustin, R.M.; Power, I.M. Characterization of gas shale pore systems by porosimetry, pycnometry, surface area, and field emission scanning electron microscopy/transmission electron microscopy image analyses: Examples from the Barnett, Woodford, Haynesville, Marcellus, and Doig units. *AAPG Bull.* **2012**, *96*, 1099–1119.
43. Clarkson, C.R.; Solano, N.; Bustin, R.M.; Bustin, A.M.M.; Chalmers, G.R.L.; He, L.; Melnichenko, Y.B.; Radliński, A.P.; Blach, T.P. Pore structure characterization of North American shale gas reservoirs using USANS/SANS, gas adsorption, and mercury intrusion. *Fuel* **2013**, *103*, 606–616. [CrossRef]
44. Loucks, R.G.; Reed, R.M.; Ruppel, S.C.; Hammes, U. Spectrum of pore types and networks in mudrocks and a descriptive classification for matrix-related mudrock pores. *AAPG Bull.* **2012**, *96*, 1071–1098. [CrossRef]
45. Kuila, U.; Prasad, M. Specific surface area and pore-size distribution in clays and shales. *Geophys. Prospect.* **2013**, *61*, 341–362. [CrossRef]
46. Mastalerz, M.; Schimmelmann, A.; Drobniak, A.; Chen, Y. Porosity of Devonian and Mississippian New Albany Shale across a maturation gradient: Insights from organic petrology, gas adsorption, and mercury intrusion. *AAPG Bull.* **2013**, *97*, 1621–1643. [CrossRef]
47. Liu, G.; Zhang, H. *Petroleum Geology*, 4th ed.; Petroleum Industry Press: Beijing, China, 2009. (In Chinese)
48. The Division of Diagenetic Stages in Clastic Rocks. In *Chinese Oil and Gas Industry Standard*; State Economic and Trade Commission: Beijing, China, 2003. (In Chinese)
49. Peters, K.E.; Cassa, M.R. Applied source rock geochemistry: Chapter 5. *AAPG Mem.* **1994**, *60*, 93–120.
50. Zhao, W.; Zhang, S.; Wang, F.; Cramer, B.; Chen, J.; Sun, Y.; Zhang, B.; Zhao, M. Gas systems in the Kuche Depression of the Tarim Basin: Source rock distributions, generation kinetics and gas accumulation history. *Org. Geochem.* **2005**, *36*, 1583–1601. [CrossRef]
51. Wei, L.; Mastalerz, M.; Schimmelmann, A.; Chen, Y. Influence of Soxhlet-extractable bitumen and oil on porosity in thermally maturing organic-rich shales. *Int. J. Coal Geol.* **2014**, *132*, 38–50. [CrossRef]

52. Löhr, S.C.; Baruch, E.T.; Hall, P.A.; Kennedy, M.J. Is organic pore development in gas shales influenced by the primary porosity and structure of thermally immature organic matter? *Org. Geochem.* **2015**, *87*, 119–132. [CrossRef]
53. Bentabol, M.; Cruz, M.D.R.; Huertas, F.J.; Linares, J. Chemical and structural variability of illitic phases formed from kaolinite in hydrothermal conditions. *Appl. Clay Sci.* **2006**, *32*, 111–124. [CrossRef]
54. Chen, J.; Xiao, X. Evolution of nanoporosity in organic-rich shales during thermal maturation. *Fuel* **2014**, *129*, 173–181. [CrossRef]
55. Bernard, S.; Wirth, R.; Schreiber, A.; Schulz, H.M.; Horsfield, B. Formation of nanoporous pyrobitumen residues during maturation of the Barnett Shale (Fort Worth Basin). *Int. J. Coal Geol.* **2012**, *103*, 3–11. [CrossRef]
56. Gai, H.; Xiao, X.; Cheng, P.; Tian, H.; Fu, J. Gas generation of shale organic matter with different contents of residual oil based on a pyrolysis experiment. *Org. Geochem.* **2015**, *78*, 69–78. [CrossRef]
57. Liu, Y.; Xiong, Y.; Li, Y.; Peng, P. Effects of oil expulsion and pressure on nanopore development in highly mature shale: Evidence from a pyrolysis study of the Eocene Maoming oil shale, south China. *Mar. Pet. Geol.* **2017**, *86*, 526–536. [CrossRef]
58. Klaver, J.; Desbois, G.; Littke, R.; Urai, J.L. BIB-SEM pore characterization of mature and post mature Posidonia Shale samples from the Hils area, Germany. *Int. J. Coal Geol.* **2016**, *158*, 78–89. [CrossRef]
59. Dias, R.F.; Freeman, K.H.; Lewan, M.D.; Franks, S.G. $\delta^{13}C$ of low-molecular-weight organic acids generated by the hydrous pyrolysis of oil-prone source rocks. *Geochim. Cosmochim. Acta* **2002**, *66*, 2755–2769. [CrossRef]
60. Baruch, E.T.; Kennedy, M.J.; Löhr, S.C.; Dewhurst, D.N. Feldspar dissolution-enhanced porosity in Paleoproterozoic shale reservoir facies from the Barney Creek Formation (McArthur Basin, Australia). *AAPG Bull.* **2015**, *99*, 1745–1770. [CrossRef]
61. Huang, S.J.; Huang, K.K.; Feng, W.L.; Tong, H.P.; Liu, L.H.; Zhang, X.H. Mass exchanges among feldspar, kaolinite and illite and their influences on secondary porosity formation in clastic diagenesis-a case study on the Upper Paleozoic, Ordos Basin and Xujiahe Formation, western Sichuan depression. *Geochimica* **2009**, *38*, 498–506, (In Chinese with English abstract).
62. Hu, H.; Hao, F.; Lin, J.; Lu, Y.; Ma, Y.; Li, Q. Organic matter-hosted pore system in the Wufeng-Longmaxi (O_3w-$S_1$1) shale, Jiaoshiba area, Eastern Sichuan Basin, China. *Int. J. Coal Geol.* **2017**, *173*, 40–50. [CrossRef]
63. Surdam, R.C.; Crossey, L.J.; Eglinton, G.; Durand, B.; Pigott, J.D.; Raiswell, R.; Berner, R.A. Organic-inorganic reactions during progressive burial: Key to porosity and permeability enhancement and preservation [and discussion]. *Philos. Trans. R. Soc.* **1985**, *315*, 135–156.
64. Saffer, D.M.; Marone, C. Comparison of smectite-and illite-rich gouge frictional properties: Application to the updip limit of the seismogenic zone along subduction megathrusts. *Earth Planet Sci. Lett.* **2003**, *215*, 219–235. [CrossRef]
65. Lee, S.; Fischer, T.B.; Stokes, M.R.; Klingler, R.J.; Ilavsky, J.; McCarty, D.K.; Wigand, M.O.; Derkowski, A.; Winans, R. Dehydration effect on the pore size, porosity, and fractal parameters of shale rocks: Ultrasmall-angle X-ray scattering study. *Energy Fuels* **2014**, *28*, 6772–6779. [CrossRef]